

# Splashing of liquids: interplay of surface roughness with surrounding gas

Lei Xu, Loreto Barcos, and Sidney R. Nagel

*The James Franck Institute and Department of Physics,  
The University of Chicago, 929 East 57th St., Chicago, Illinois 60637*

(Dated: June 28, 2021)

We investigate the interplay between substrate roughness and surrounding gas pressure in controlling the dynamics of splashing when a liquid drop hits a dry solid surface. We associate two distinct forms of splashing with each of these control parameters: prompt splashing is due to surface roughness and corona splashing is due to instabilities produced by the surrounding gas. The size distribution of ejected droplets reveals the length scales of the underlying droplet-creation process in both cases.

PACS numbers: 47.55.Dz, 47.20.Cq, 47.20.Ma

## I. Two contributions to splashing

A liquid drop hitting a surface will often splash, rupturing into many tiny droplets. Although splashing is ubiquitous and important in many applications [1, 2, 3], the control parameters governing its occurrence have not yet been fully explored. Impact velocity, surface tension, viscosity and substrate roughness have long been known to be important [4, 5, 6]. However only recently was it discovered that splashing can be completely eliminated on smooth surfaces simply by lowering the surrounding gas pressure [7]. In this paper we focus on the role that surface roughness plays in producing a splash. Given the discovery that the gas pressure can, by itself, cause splashing, it is apparent that only by removing the surrounding gas can the other control parameters, such as surface roughness, be investigated in isolation. In order to make progress, we therefore eliminate all vestiges of the corona splash by working at low gas pressures. This insures that the effects of surface roughness are unperturbed by the effects of the surrounding gas.

Two types of splashing are well-known in the literature [8]: “corona” splashing, where a corona forms and subsequently ruptures and “prompt” splashing, where droplets emerge at the advancing liquid-substrate contact line. Although the two phenomena are distinct there has been no fundamental understanding of their separate causes. The results reported here suggest a simple explanation: corona splashing is due to the presence of surrounding gas and occurs above a critical gas pressure and prompt splashing occurs on rough surfaces even in the absence of air. By studying the ejected-droplet size distribution of these two forms of splashing, we can determine the characteristic length scale of the droplet-creation process in each case. This corroborates our interpretation of how the splash is formed.

Our previous experiment [7] clearly showed that surrounding gas causes the corona splash on smooth surfaces. Here we study the effect of another control parameter: surface roughness. In order to do this cleanly, we must lower the gas pressure until the effects of air are negligible. We achieved this by doing an experiment in a helium atmosphere at 13kPa pressure, much lower

than the threshold pressure [7] for the surrounding gas to produce a corona splash. In this situation, therefore, splashing is caused entirely by surface roughness.

In our experiments, we use ethanol which has density  $\rho = 0.789\text{g/cm}^3$ , viscosity  $\nu = 1.36\text{cSt}$  and surface tension  $\sigma = 22\text{mN/m}$ . We filmed drops, of diameter  $D = 3.4 \pm 0.1\text{mm}$ , released inside a transparent vacuum chamber from a nozzle at a height 95 cm above a rough substrate. The impact speed of the drop,  $V_0 = 4.3 \pm 0.1\text{m/s}$ , was determined by analyzing the drop position in subsequent frames of each movie. Rough substrates were obtained by using high-quality sandpapers uniformly coated with closely packed particles (*microcut-paper-discs*<sup>®</sup>, Buehler Ltd.). The roughness,  $R_a$ , defined as the average diameter of the particles, was varied between  $3\mu\text{m}$  and  $78\mu\text{m}$ . Clean glass microscope slides were used as the smooth substrates. The gas pressure,  $P$ , was varied. Ethanol wets our substrates and does not rebound after hitting the surface [9]. We also note that although ethanol wets the substrate (zero degree static contact angle), the profile of the liquid film during expansion has a finite thickness at the edge, instead of decreasing smoothly to zero. All experiments were done at constant temperature,  $23.6^\circ\text{C}$ .

As we increase the roughness,  $R_a$ , we see an evolution in behavior as shown in Fig. 1. We compare the splash created solely by surface roughness at low pressure with the splash created when air is also present. In each panel the top row is at low pressure,  $P = 13\text{kPa}$ , and the bottom row is at atmospheric pressure,  $P = 100\text{kPa}$ . Fig. 1a shows the result for a smooth surface: at low pressure there is only a liquid film expanding smoothly on the substrate with no splashing whereas at atmospheric pressure there is a corona that breaks up into many small droplets. This shows unambiguously that air causes corona splashing. Fig. 1b shows the result for a small amount of roughness,  $R_a = 5\mu\text{m}$ . In this case, at low  $P$  there are two regimes: an early stage with prompt splashing which is followed by a peaceful regime where no splashing occurs. At atmospheric pressure, there is a single regime throughout the expansion that resembles corona splashing except that it is not as symmetric as when the surface is completely smooth. Thus, for roughness  $R_a = 5\mu\text{m}$ ,

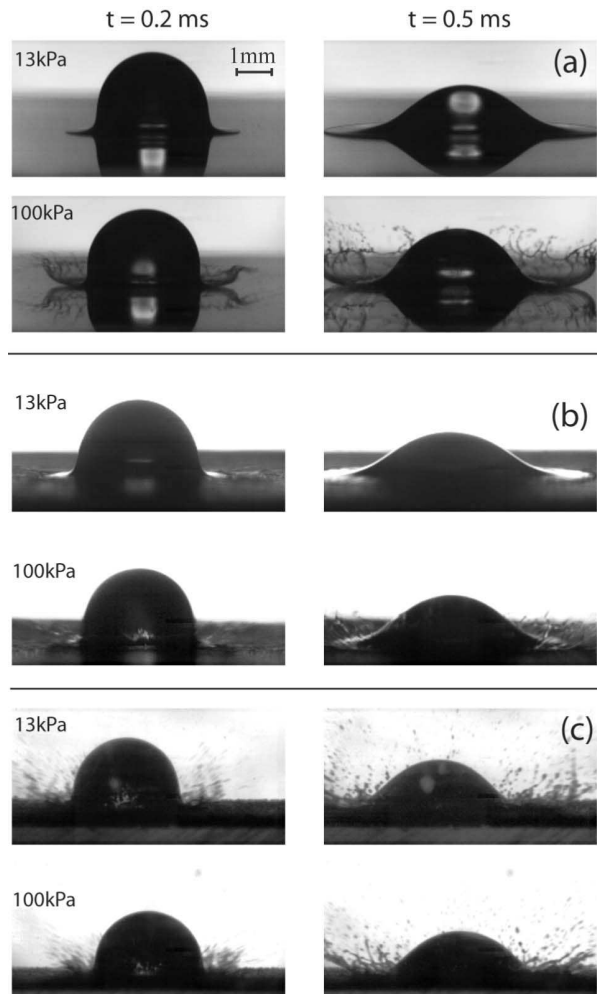


FIG. 1: Photographs of splashing as a function of gas pressure and surface roughness. The left and right columns are 0.2 ms and 0.5 ms from the time of impact. For each value of surface roughness, the top panel is at a low pressure,  $P = 13 \text{ kPa}$  and the bottom panel is at atmospheric pressure,  $P = 100 \text{ kPa}$ . (a) Splash on a smooth substrate which is a clean microscope slide. (b) Splash on a substrate with roughness  $R_a = 5 \mu\text{m}$ . (c) Splash on a substrate with roughness  $R_a = 78 \mu\text{m}$ .

there is a clear difference as  $P$  is increased, showing that surrounding gas can still be important at atmospheric pressure. For large roughness,  $R_a = 78 \mu\text{m}$ , we see typical prompt splashing, where droplets are ejected from the expanding contact line during the entire expanding process for both low and atmospheric pressures.

In summary, there are two contributions to splashing: a corona part caused by gas and a prompt part caused by surface roughness. At low pressures, for small roughness ( $R_a = 5 \mu\text{m}$ ), there is no corona and there is only a small amount of prompt splashing produced at the beginning. This prompt splashing disappears at later times. For large roughness ( $R_a = 78 \mu\text{m}$ ), splashing at the advancing contact line is produced throughout the entire duration of the expansion. At atmospheric pressure there is a tran-

sition as the roughness is increased: the corona splash dominates at small surface roughness and the prompt splash dominates at large  $R_a$ .

These results indicate that in the absence of air, splashing is caused when the expanding liquid film, of thickness  $d$ , becomes destabilized by surface roughness; but if the roughness is too small or the film is too thick then no splashing will occur. Initially the expanding film thickness  $d$  is of molecular size and increases in thickness during expansion as liquid is added to the film. Thus for small roughness ( $R_a = 5 \mu\text{m}$ ), splashing occurs immediately after impact and is followed by a quiescent stage as the film becomes much thicker than the roughness. For large roughness ( $78 \mu\text{m}$ ), splashing continues throughout the film expansion since  $d$  never grows large enough to be unperturbed by the roughness. From the photographs, we estimated the liquid film thickness,  $d$ , at the point where splashing stops for  $R_a = 5 \mu\text{m}$  and found  $d \sim 50 \mu\text{m}$ . This suggests the following criterion for prompt splashing:

$$\frac{R_a}{d} = C(We, Re) \quad (1)$$

where  $C(We, Re)$  is a dimensionless number depending on Weber number  $We = \rho V_0^2 D / \sigma$  and Reynolds number  $Re = \rho V_0 D / \mu$ . For the impact conditions in Fig. 1,  $We \approx 2400$  and  $Re \approx 11500$ , we conclude  $C \sim 0.1$ . Further studies are necessary to establish the dependence of  $C$  on  $We$  and  $Re$ . For example, at sufficiently low velocity we might not expect to see any splash at all. We emphasize that  $C(We, Re)$  can only be measured accurately when the effect of gas pressure is negligible since otherwise the corona component will contaminate the results. This shows the importance of separating the two types of splashing by working at small  $P$ .

## II. Size distribution of prompt splashing

After impact, the liquid breaks up into many tiny droplets. The size distribution of these emitted droplets,  $N(r)$ , may retain an imprint of the droplet creation process and thus provide a clue to the mechanism initiating the interfacial instability. Here we report  $N(r)$  for prompt splashing on rough substrates.

We measure the size of emitted droplets by adding a small amount of ink (*Sanford*<sup>®</sup> black stamp pad ink) to the ethanol, at the volume ratio 1:6 (ink:ethanol). The mixed liquid has the following material properties: density:  $\rho = 0.833 \pm 0.002 \text{ g/cm}^3$ , viscosity:  $\nu = 3.4 \pm 0.2 \text{ cSt}$ , surface tension:  $\sigma = 23 \pm 3 \text{ mN/m}$ . ( $\sigma$  is measured both in air and helium atmosphere under low pressure. Both cases give the same result,  $23 \pm 3 \text{ mN/m}$ .) Except for the viscosity, which increases by a factor of 2.5, these values are close to those for pure ethanol. We have also checked repeatedly with high-speed video and found that the splashing pictures look very similar with and without ink, therefore we made sure that the addition of ink does not change splashing qualitatively. We surround the

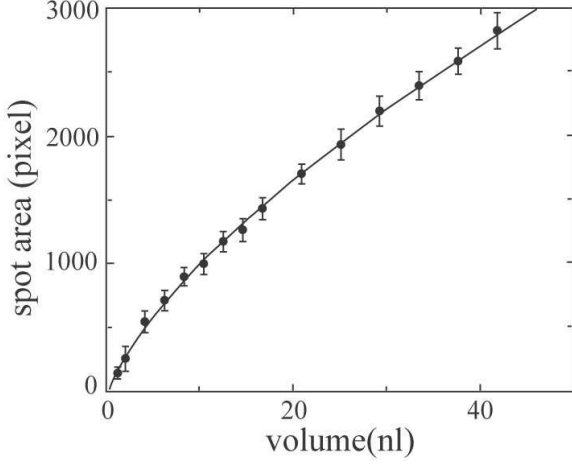


FIG. 2: Calibration curve of stain area as function of droplet volume. Error bars come from the fluctuation of stain areas for the same size droplet. The fitting curve is:  $y = 233 * x^{0.67} - 119$ .  $y$  is the stain area in units of pixels, and  $x$  is the volume of the drop in units of nanoliters.

impact point with a cylinder of diameter  $8.89 \pm 0.02 \text{ cm}$  rolled from a sheet of white paper. After splashing, the droplets hit the cylinder, leaving stains.

With careful calibration, we convert the sizes of the ink spots on the paper to the sizes of the ejected droplets. Our calibrations work well for drops with radius larger than  $r = 50 \mu\text{m}$ . Below that radius, our resolution is inadequate to obtain a reliable calibration. We used a  $0.5 \mu\text{l}$  syringe to deliver tiny droplets of the ethanol/ink fluid with known volume to white paper. By measuring the area of the stains created by these droplets we obtained the calibration curve in Fig. 2. We checked the effect of droplet velocity on the stain area and found no significant effect within our experimental accuracy. By checking the shape of a stain, we can ascertain whether that spot was caused by a single ejectile or by two separate drops that landed in overlapping locations. We found less than 4% overlapping stains. We excluded them from our distribution curves.

We first determine  $N(r)$  for prompt splashing on rough substrates. To ensure that these distributions are due solely to prompt splashing, we performed the measurements at low pressure. Fig. 3a shows  $N(r)$  for several values of roughness,  $R_a$ . To obtain good statistics, each distribution is an average over ten to twenty experiments taken under the same conditions. We added the number of spots found in all the experiments and then divided the total counts by the number of experiments. The straight lines in the figure indicate that  $N(r)$  decays exponentially with a characteristic decay length,  $r_0$ :

$$N \sim \exp(-r/r_0) \quad (2)$$

Fig. 3b shows that the decay length of these lines,  $r_0$ , increases with increasing  $R_a$ . At small  $R_a$ , the decay

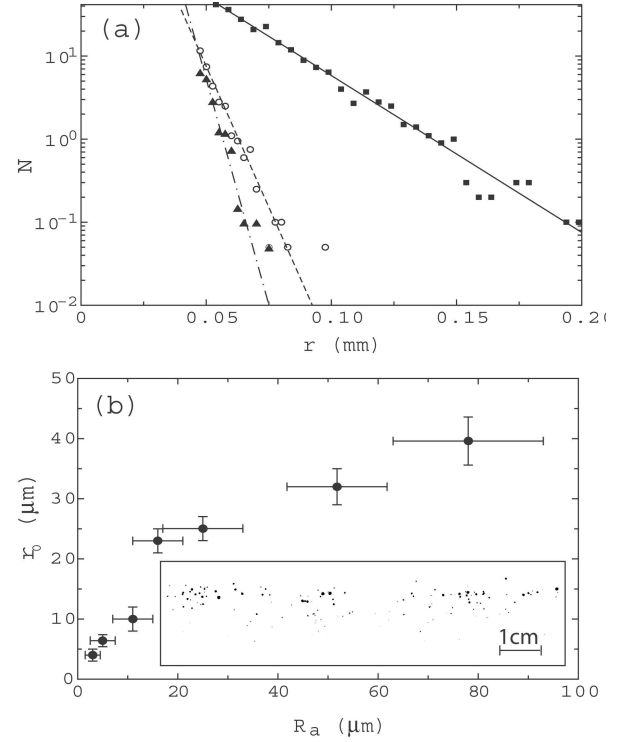


FIG. 3: The distribution of ejected drops in a prompt splash on rough substrates. (a)  $N(r)$  versus  $r$  for splashes on substrates with three values of roughness:  $R_a = 16 \mu\text{m}$  (■),  $R_a = 5 \mu\text{m}$  (○), and  $R_a = 3 \mu\text{m}$  (▲). The exponential fitting functions are: —,  $\exp(-r/0.023)$ ; ---,  $\exp(-r/0.006)$ ; and -·-,  $\exp(-r/0.004)$ . (b) The decay constant,  $r_0$ , of the exponential decay in  $N(r)$ , as a function of substrate roughness  $R_a$ . For small values of roughness, the decay constant is approximately linear in the roughness. At large roughness, the decay constant saturates. The sizes of particles on sandpaper are randomly distributed around an average value,  $R_a$ . The fluctuation of particle sizes gives us  $R_a$  error bars; and the standard deviation from exponential fit gives the  $r_0$  error bars. Inset of (b) shows one sheet of paper with ink spots produced by  $R_a = 25 \mu\text{m}$ . Most spots are randomly distributed within a narrow band.

length is close to the value of the roughness:  $r_0 \approx R_a$ . At large roughness, this relationship breaks down as  $r_0$  appears to saturate at a constant value.

This behavior is consistent with the prompt splashing criteria, Eq. 1. When the roughness is small, the drop stops splashing at a film thickness determined by  $R_a$ . This sets the correlation between the droplet decay length and roughness:  $r_0 \approx R_a$ . However, when the roughness is too large, the drop never stops splashing, and  $r_0$  can only increase up to the maximum thickness of the expanding liquid film. From the photographs we estimate thickness  $d \sim 100 \mu\text{m}$ . Fig. 3b shows that the saturation occurs at approximately  $40 \mu\text{m}$ , which is about the same order of magnitude as the thickness of the liquid film at its terminal position.

How robust is the decay length,  $r_0$ , with respect

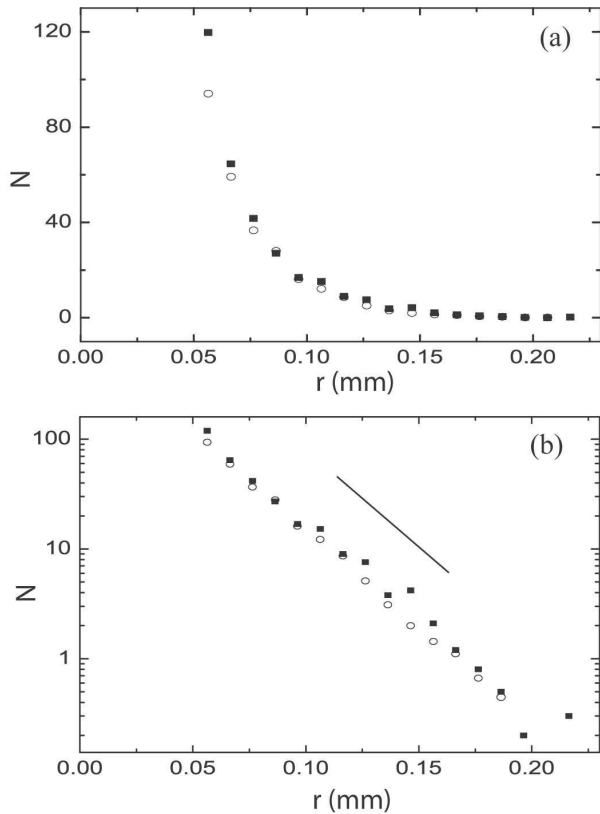


FIG. 4: Size distribution of different impact velocities. For a fixed roughness  $R_a = 25 \mu\text{m}$ , two impact velocities were tested:  $V_0 = 4.3 \pm 0.1 \text{ m/s}$  (○) and  $V_0 = 5.2 \pm 0.1 \text{ m/s}$  (■). (a) shows  $N(r)$  in linear-linear scale. It's clear that the higher velocity case produces about 20% more splash. (b) plots the same data in log-linear format. The two data sets now seem much closer only because of the log-linear way we plot them. We can fit both curves with the same functional form:  $A \cdot \exp(-r/0.025)$  (the solid line), by only varying the amplitude,  $A$ . This implies that  $r_0 = 0.025 \text{ mm}$  is independent of impact velocity.

to variations of the impact velocity  $V_0$ , drop size  $R$ , or surface tension  $\sigma$ ? In Fig. 4 we show the size distribution for two different impact velocities:  $V_0 = 4.3 \pm 0.1 \text{ m/s}$  ( $We = 2155$ ,  $Re = 3648$ ) and  $V_0 = 5.2 \pm 0.1 \text{ m/s}$  ( $We = 3151$ ,  $Re = 4412$ ). Fig. 4(a) shows that there is significantly more splashing at higher impact velocity. Fig. 4(b) plots the same data in log-linear format and shows that both curves can be fitted by straight lines with the same decay length,  $r_0$ . This implies that  $r_0$  is independent of  $V_0$ . Further experiments addressing other parameters should be done in the future. Although the absolute value of  $r_0$  might change with those parameters, we expect that the two general features: (1) the distribution decays exponentially and (2)  $r_0$  increases with surface roughness, would still be valid.

### III. Size distribution of corona splashing

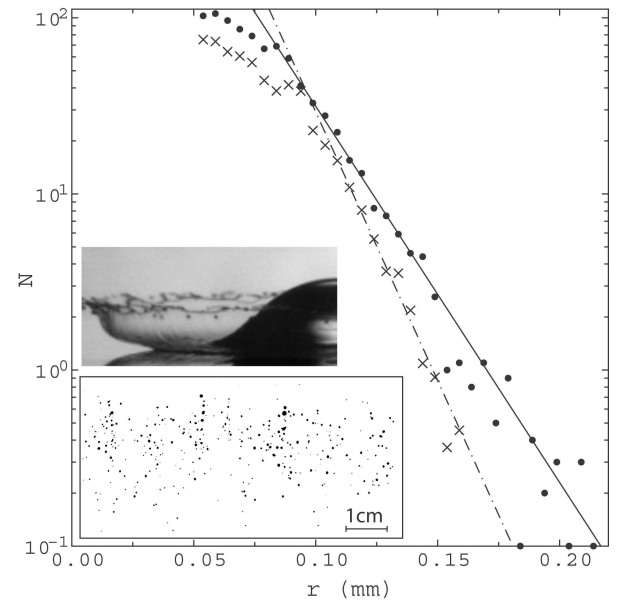


FIG. 5: Size distribution of ejected droplets in a corona splash at high pressure. Upper inset shows the corona film before it breaks up. From this picture we can estimate the film thickness to be  $20 \sim 40 \mu\text{m}$  by measuring the thickness of the corona rim. (Although rim should be thicker than the film, we assume that the film and the rim are approximately the same size.) Lower inset is a reproduction of the sheet of paper with the ink spots showing that the ejected droplets hit the paper at random locations over a large area. Main panel shows the number of droplets of a given size per impact,  $N(r)$ , versus droplet radius,  $r$ , for a corona splash at two pressures:  $P = 100 \text{ kPa}$  (●) and  $P = 80 \text{ kPa}$  (×). The exponential fitting functions are respectively: —,  $\exp(-r/0.020)$ ; and - - -,  $\exp(-r/0.014)$ .

We have also performed measurements of the size distributions produced in a corona splash. This allows us to compare prompt and corona splashing. Fig. 5 shows the results of splashing on a smooth surface at two pressures, 100 kPa and 80 kPa, both in the high pressure regime. The inset shows the spots created by the droplets ejected from a single splash. The spots are randomly distributed. The main panel shows the distribution of droplet sizes,  $N(r)$ , for the two pressures. We again see an exponential distribution at large radius  $r$ ,  $N \sim \exp(-r/r_0)$ , indicating the existence of a characteristic length scale. The values we find for  $r_0$  (given in the caption of Fig. 5) are comparable to the corona thickness which we estimated from the movies to be between 20 and  $40 \mu\text{m}$ . (The corona thickness was estimated by measuring the edge of the corona in pictures similar to the one shown in the inset to Fig. 5.) This suggests that the corona thickness determines  $r_0$ . That  $r_0$  decreases as the pressure decreases suggests that lower pressure leads to less splashing and a thinner corona. The data in Fig. 5 shows that the size-distribution data can probe the slight differences in the

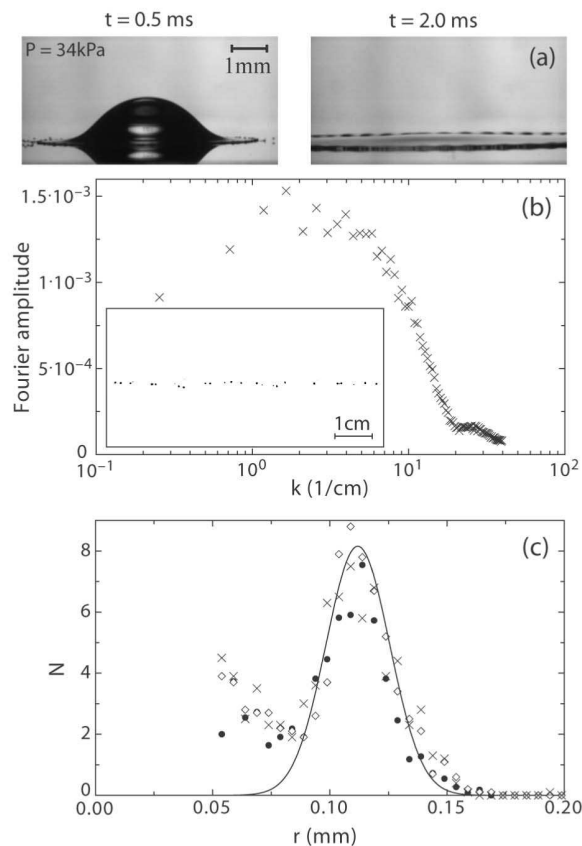


FIG. 6: A splash just above the threshold pressure,  $P_T$ . (a) Images of a drop splashing show the ejection of droplets and the undulations in the expanding rim. The times shown are measured with respect to the time of impact. (b) Inset is a reproduction of the sheet of paper showing that the droplets hit the paper in a well-defined horizontal line. Main panel of (b) shows the Fourier transform of the lateral positions of the spots in the inset. The peak indicates a well-defined spacing between the ejected droplets at  $P_T$ . (c) The number of droplets at fixed sizes,  $N(r)$ , is plotted versus droplet radius,  $r$ , at pressures slightly higher than  $P_T$ :  $P = 34$  kPa ( $\bullet$ ),  $P = 37$  kPa ( $\circ$ ) and  $P = 39$  kPa ( $\times$ ). The solid line is a Gaussian fit centered at  $r_0 = 0.11$  mm. The peak in  $N(r)$  shows that the average size of the droplets is approximately the size of the undulations at the rim of the expanding film.

corona formed at the two pressures.

Both prompt and corona splashing have exponential distributions for  $N(r)$ . Although there is a characteristic length scale in both cases, the control parameters

governing the length scales are different: roughness in Fig. 3 and gas pressure in Fig. 5. However, at the threshold pressure [7] for the corona splash on a smooth surface, there is a qualitatively different distribution of droplet sizes. Fig. 6a shows there is no corona and that discrete droplets emerge from the expanding liquid which has periodic undulations along its rim. The ink spots shown in the inset at the lower left corner of Fig. 6b have the striking feature that they fall in a horizontal line, indicating that the ejected droplets have the same angle between their trajectories and the substrate. In addition, the spots are approximately equally spaced. The main panel of Fig. 6b shows that the Fourier transform of the lateral positions of the spots has a peak indicating this spatial order. Moreover the spot sizes are more uniform than those seen at high pressures in the inset to Fig. 5. Fig. 6c shows  $N(r)$  at pressures close to  $P_T$ . The peak at  $r_0 = 0.11$  mm indicates that most droplets are about the size of the rim undulations.

#### IV. Conclusions

By controlling the gas pressure and surface roughness we have identified two mechanisms for splashing: the surrounding gas is responsible for corona splashing and surface roughness is responsible for prompt splashing. This explains the long-standing puzzle about why two distinct types of splashes exist. We have also found that there are characteristic lengths in the distribution of ejected drops in both cases. Similar exponential dependence is found in ligament breakup, implying a possible connection with that process[10, 11]. However, the exponential dependence of droplet sizes found in the splashing of liquids is in contrast to what is found in the shattering of a solid. In that case, there is a power-law distribution of sizes of the shattered fragments and no characteristic length scale[12, 13]. The characteristic lengths we find in liquid splashing experiments reveal the microscopic length scales associated with the droplet creation process. On rough surfaces, the length scales we determine are consistent with our interpretation of the prompt splash in terms of the surface roughness. These results also suggest a means for controlling the sizes of ejected droplets in a splash.

**Acknowledgement** We wish to thank Qiti Guo, Priyanka Jindal, David Qu  r  , Mathilde Callies-Reyssat, and Wendy Zhang for helpful discussions. This work was supported by MRSEC DMR-0213745 and NSF DMR-0652269.

[1] S. Sampath, X. Y. Jiang, J. Matejcek, A. C. Leger and A. Vardelle, *Mater. Sci. Eng. A* **272**, 181 (1999).  
 [2] K.R. Koederitz, M.R. Evers, G.B. Wilkinson and J.A. Drallmeier, *Int. J. Engine Research* **3**, 37 (2003).  
 [3] F.V. Shaw, *Ceramic Bulletin* **69**, 1484 (1990).

[4] A.M. Worthington, *Proc. R. Soc. Lond.* **25**, 261 (1876-1877).  
 [5] C. Mundo, M. Sommerfeld and C. Tropea, *Int. J. Multiphase Flow* **21**, 151 (1995).  
 [6] K. Range and F. Feuillebois, *J. Colloid Interface Sci.* **203**,

- 16 (1998).
- [7] L. Xu, W. W. Zhang and S. R. Nagel, Phys. Rev. Lett. **94**, 184505 (2005).
- [8] R. Rioboo, M. Marengo and C. Tropea, Atomization and Sprays **11**, 155 (2001).
- [9] D. Richard, C. Clanet and D. Quéré, Nature **417**, 811 (2002).
- [10] P. Marmottant and E. Villermaux, J. Fluid Mech. **498**, 73 (2004).
- [11] E. Villermaux, P. Marmottant and J. Duplat, Phys. Rev. Lett. **92**, 074501 (2004).
- [12] L. Oddershede, P. Dimon and J. Bohr, Phys. Rev. Lett. **71**, 3107 (1993).
- [13] A. Meibom and I. Balslev, Phys. Rev. Lett. **76**, 2492 (1996).